Electronic structure study of wide band gap magnetic semiconductor (La0.6Pr0.4)0.65Ca0.35MnO3 nanocrystals in paramagnetic and ferromagnetic phases

G. D. Dwivedi, Amish G. Joshi, Shiv Kumar, H. Chou, K. S. Yang, D. J. Jhong, W. L. Chan, A. K. Ghosh, and Sandip Chatterjee

Articles you may be interested in

Magnetic properties and X-ray absorption spectra of La0.7Ca0.3MnO3 nanoparticles
J. Appl. Phys. **113**, 17E101 (2013); 10.1063/1.4793514

Exchange bias and enhanced coercivity in phase separated La0.45Sr0.55MnO3 and Pr0.55(Ca0.65S0.35)0.45MnO3 films
J. Appl. Phys. **110**, 123907 (2011); 10.1063/1.3666023

Large reversible magnetocaloric effect in La0.7-xPrxCa0.3MnO3
J. Appl. Phys. **110**, 013906 (2011); 10.1063/1.3603014

Collapse of charge ordering and enhancement of magnetocaloric effect in nanocrystalline La 0.35 Pr 0.275 Ca 0.375 MnO 3
Appl. Phys. Lett. **97**, 242506 (2010); 10.1063/1.3526380

Influence of structural disorder on magnetic and transport properties of (La 0.7 Sr 0.3) 0.5 (Pr 0.65 Ca 0.35) 0.5 MnO 3 films
Low Temp. Phys. **31**, 161 (2005); 10.1063/1.1820566

Electronic structure study of wide band gap magnetic semiconductor (La$_{0.6}$Pr$_{0.4}$)$_{0.65}$Ca$_{0.35}$MnO$_3$ nanocrystals in paramagnetic and ferromagnetic phases

G. D. Dwivedi,[1] Amish G. Joshi,[2] Shiv Kumar,[3] H. Chou,[1] K. S. Yang,[1] D. J. Jhong,[1] W. L. Chan,[1] A. K. Ghosh,[3] and Sandip Chatterjee[4,a)]

[1]*Department of Physics, National Sun Yat-sen University, Kaohsiung 80424, Taiwan*
[2]*CSIR-National Physical Laboratory, Dr. K. S. Krishnan Road, New Delhi 110012, India*
[3]*Department of Physics, Banaras Hindu University, Varanasi 221005, India*
[4]*Department of Physics, Indian Institute of Technology (Banaras Hindu University), Varanasi 221005, India*

X-ray circular magnetic dichroism (XMCD), X-ray photoemission spectroscopy (XPS), and ultraviolet photoemission spectroscopy (UPS) techniques were used to study the electronic structure of nanocrystalline (La$_{0.6}$Pr$_{0.4}$)$_{0.65}$Ca$_{0.35}$MnO$_3$ near Fermi-level. XMCD results indicate that Mn^{3+} and Mn^{4+} spins are aligned parallel to each other at 20 K. The low M-H hysteresis curve measured at 5 K confirms ferromagnetic ordering in the (La$_{0.6}$Pr$_{0.4}$)$_{0.65}$Ca$_{0.35}$MnO$_3$ system. The low temperature valence band XPS indicates that coupling between Mn3d and O2p is enhanced and the electronic states near Fermi-level have been suppressed below T$_C$. The valence band UPS also confirms the suppression of electronic states near Fermi-level below Curie temperature. UPS near Fermi-edge shows that the electronic states are almost absent below 0.5 eV (at 300 K) and 1 eV (at 115 K). This absence clearly demonstrates the existence of a wide band-gap in the system since, for hole-doped semiconductors, the Fermi-level resides just above the valence band maximum. *Published by AIP Publishing.*
[http://dx.doi.org/10.1063/1.4947466]

Perovskite manganite materials have attracted the attention of researchers due to their wide range of properties and application possibilities.[1–7] The physical properties of manganites (R$_{1-x}$A$_x$MnO$_3$, where R is a trivalent-rare earth ion and A is a divalent-alkaline earth ion) can be tuned either by changing the concentration and nature of the R and A cations[8,9] or by applying external factors such as pressure,[10–14] magnetic field,[15–17] or electric field.[18–20] All these factors can modify the physical properties of manganites by altering the electronic structure of the systems. The change in the internal structure, such as Mn^{3+}/Mn^{4+} ratio, lattice distortion, and spin state, varies the electronic occupation at the Mn site and the lattice distortion, which controls the band filling and e$_g$ bandwidth, hence influencing the electronic properties of manganites. A recent study of (La$_{0.6}$Pr$_{0.4}$)$_{0.65}$Ca$_{0.35}$MnO$_3$ (LPCMO) nanoparticles suggests improved application possibilities for manganite materials as wide band-gap magnetic semiconductors and optoelectronic materials due to the coexistence of three features: (1) a Curie temperature (T$_C$) around 200 K, (2) a metal-insulator transition around 66–109 K, depending on the particle size, and (3) an optical band-gap of around 3.4–3.5 eV.[21] Previously reported band-gaps for manganites are well below the band-gap observed in this system.[22,23]

It is well-known that La$_{0.65}$Ca$_{0.35}$MnO$_3$ is a metallic ferromagnet below 265 K.[9,24] With doping of Pr- at the La-site, the behavior of the system changes from metallic to semiconductor, which might be due to induced charge-ordering of Mn^{3+} and Mn^{4+}. In nano-regimes, the charge-ordering is less prominent, while the grain boundary condition increases the semiconducting nature of the system. It was observed that with increasing particle size, the grain boundaries decrease and the charge-ordering increases. These factors will affect the system in two opposite ways, which give rise to competition between these two factors. This competition does not allow systems to significantly change their transport behavior, and these systems remained semiconducting up to nearly 66–109 K.[21]

The electronic states close to the Fermi-level govern the magnetic and electronic properties of the materials. Hence, the wide optical band-gap observed in (La$_{0.6}$Pr$_{0.4}$)$_{0.65}$Ca$_{0.35}$MnO$_3$ (abbreviated as LPCMO) nanocrystals demands a detailed investigation of the electronic structures near the Fermi-level to better understand this behavior. In this manuscript, we investigate the electronic states of LPCMO nanocrystals at room temperature and below Curie temperature (T$_C$) by X-ray magnetic circular dichroism (XMCD), X-ray photoemission spectroscopy (XPS), and ultraviolet photoemission spectroscopy (UPS). The XMCD result shows that Mn^{3+} and Mn^{4+} spins are aligned parallel to each other at 20 K. The valence band XPS and UPS shows that the electronic states near the Fermi-level have been suppressed in the ferromagnetic state. UPS in the vicinity of the Fermi-level confirms the existence of a wide band-gap in the LPCMO nanocrystals. This result establishes that magnetic manganite systems are indeed wide band-gap semiconductors, which can prove beneficial in spintronic device applications.

(La$_{0.6}$Pr$_{0.4}$)$_{0.65}$Ca$_{0.35}$MnO$_3$ (LPCMO) nanocrystals were synthesized via the sol-gel reaction technique. The details of sample synthesis process and characterization results (structural, magnetic, transport, and optical properties) have been previously reported.[21] For the electronic structure study, the

---

a)Author to whom correspondence should be addressed. Electronic mail: schatterji.app@iitbhu.ac.in

LPCMO nanocrystals sintered at 800 °C were used as a representative. XMCD measurements in the total electron yield (TEY) mode were done at the National Synchrotron Radiation Research Centre (NSRRC), Taiwan, in the 11A1 beamline on the Mn$L_{2,3}$-edge. Photon energy resolution and data cumulative time were set at 0.1 eV and 1 s, respectively. The room temperature and low temperature X-ray photoemission spectroscopy measurements were done using an Omicron multiprobe surface analysis system operating at an average base pressure of $\sim 5 \times 10^{-10}$ Torr with a monochromatic AlK$_\alpha$ line at 1486.70 eV. The total energy resolution, estimated from the width of the Fermi-edge, was about 0.25 eV for the monochromatic AlK$_\alpha$ line with photon energy 1486.70 eV. During photoemission experiment, due to specimen charging, carbon was accumulated on the sample surface. During analysis, we calibrated all spectra positions with respect to C1s signal at 284.5 eV. Ultraviolet photoemission spectroscopy measurements were done using the non-monochromatic He I (21.2 eV) line at an average base pressure of 6.8×10^{-8} Torr. To study the fine changes near Fermi-level, Fermi-edge UPS were collected with energy resolution of the analyzer and the step size set at 0.03 eV and 0.005 eV, respectively. The low temperature measurements were carried out using an open liquid nitrogen (LN$_2$) cryostat.

To investigate the element-specific magnetic properties of LPCMO nanocrystals, we examined the XMCD at the Mn$L_{2,3}$-edge. XMCD can be used to estimate the element-specific orbital and spin angular momentum in 3d transition metals and their related compounds[25] by using simple orbital[26] and spin[27] sum rules. The XMCD signal conveys the information about orbital and spin polarizations of valence electrons. The Mn$L_{2,3}$ absorption edge arises from the excitation of electron from Mn2p core-level to Mn3d valence-level, which carries information about the valence band structure and hence about the Fermi-level. X-ray absorption spectra (XAS) at the Mn$L_{2,3}$-edge were collected in total electron yield (TEY) mode with circularly polarized photons under the applied magnetic field of +1 T and −1 T at 20 K (Fig. 1(a)). XAS spectra exhibit two broad spin-orbit splitting of peaks, those of Mn2$p_{3/2}$ (MnL_3) and Mn2$p_{1/2}$ (MnL_2). Both peaks have two distinguishable features, resembling two distinct oxidation states Mn^{3+} and Mn^{4+}. The intensity of absorption spectra depends on the number of empty d-valence states, which explain the higher intensity of Mn^{4+} in comparison to Mn^{3+}. In a magnetic material, the imbalance between spin-up and spin-down electrons of d-shell, or similarly the imbalance between spin-up and spin-down holes (with opposite sign), provides spin moment. The difference between spin-up and spin-down d-holes can be observed by making the X-ray absorption process spin dependent. This is done by using circularly polarized photons under oppositely directed applied magnetic fields, which transfer their angular momentum to the excited photoelectron. XMCD signals can be obtained from the difference in observed X-ray absorption under +1 T and −1 T applied magnetic fields (Fig. 1(b)). The XMCD signal shows significant dichroism associated with the Mn$L_{2,3}$-edge, which provides information about the magnetic characteristics of this system. The XMCD signal at the L_3-edge shows two features, one associated with Mn^{3+}
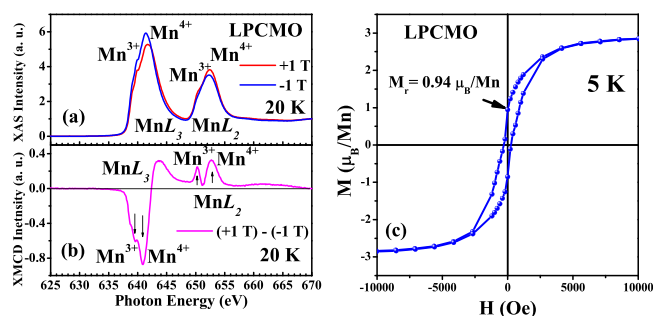

FIG. 1. (a) X-ray absorption spectra at Mn$L_{2,3}$-edge of LPCMO nanocrystals measured in the TEY mode with circularly polarized photons under applied magnetic fields of +1 T and −1 T at 20 K. (b) X-ray magnetic circular dichroism (XMCD) signal at Mn$L_{2,3}$-edge shows that Mn^{3+} and Mn^{4+} spins are aligned parallel to applied magnetic field. (c) M-H hysteresis loop of LPCMO nanocrystals measured at 5 K.

and other with Mn^{4+}. Similar, but clearly distinguished, features of Mn^{3+} and Mn^{4+} are observed at the L_2-edge. The XMCD signals of Mn^{3+} and Mn^{4+} at both edges (L_3 and L_2) confirm that spins associated with both cations are oriented parallel to the direction of the applied magnetic field. Similar XMCD features have been reported for metallic ferromagnetic La$_{0.7}$Sr$_{0.3}$MnO$_3$, La$_{0.7}$Ca$_{0.3}$MnO$_3$ thin-films and their heterostructure systems.[28–33] The XMCD signal observed at the MnL_3-edge of the present nanocrystalline LPCMO is $\sim$16%, which is smaller than the reported XMCD signals of $\sim$23% for La$_{0.7}$Sr$_{0.3}$MnO$_3$ and La$_{0.7}$Ca$_{0.3}$MnO$_3$ thin-films.[28,31–33] This decrease in XMCD signal can be understood on the basis of antiferromagnetic charge-ordering and nano-crystalline size[34] of LPCMO systems, which suppresses its magnetic properties and hence the XMCD signal. Nevertheless, this XMCD signal indicates possible ferromagnetic behavior and clearly demonstrates a parallel alignment of spin moments associated with Mn^{3+} and Mn^{4+} cations below T$_C$. To confirm the ferromagnetic behavior of the system, magnetic field dependent magnetization (M-H) measurements were performed at 5 K (Fig. 1(c)). Magnetization is almost saturated (2.85 μ_B/Mn) for 1 T magnetic field and shows remanence (M$_r$) of $\sim$0.94 μ_B/Mn. Saturation magnetization at 1 T magnetic field is less than the magnetic moment observed for La$_{0.65}$Ca$_{0.35}$MnO$_3$ systems (3.65 μ_B/Mn). This suppressed magnetization is consistent with the observed XMCD signal suppression.

To obtain information about the electronic structures of nanocrystalline LPCMO near the Fermi-level, XPS and UPS were performed at 300 K and 115 K. All the peak positions and doublet separation have been assigned from the National Institute of Standards and Technology (NIST) X-ray photoemission spectroscopy database.[35] Survey scans at both temperatures confirm the presence of La, Pr, Ca, Mn, and O on the surface of the sample (Fig. 2(a)). Figure 2(b) represents the core level XPS of the Pr3d region. At 300 K, the Pr3d region shows spin-orbit split 3$d_{5/2}$ (933.1 eV) and 3$d_{3/2}$ (953.2 eV) peaks with a doublet separation of 20.1 eV, which corresponds to a divalent (+3) state of Pr. At 115 K, doublet peaks shift 0.15 eV towards higher energy (933.25 eV and 953.35 eV). The La3d region has well-separated spin-orbit split peaks (Fig. 2(c)). The peaks between 830 eV and 840 eV correspond to La3$d_{3/2}$ and peaks from 850 eV to 860 eV
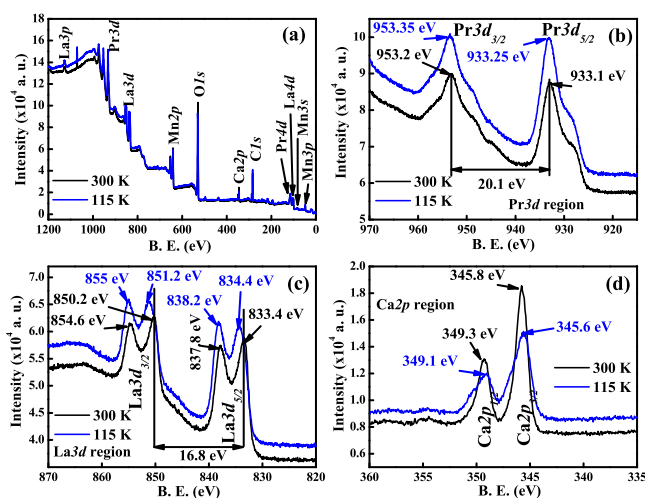
FIG. 2. (a) Survey scan, (b) Pr3*d*, (c) La3*d*, and (d) Ca2*p* core level X-ray photoemission spectra for LPCMO nanocrystals at 300 K and 115 K.

FIG. 3. (a) O1*s*, (b) Mn2*p*, (c) Mn3*s* core-level, and (d) valence band X-ray photoemission spectra for LPCMO nanocrystals at 300 K and 115 K.

correspond to La3$d_{5/2}$. Each spin-orbit split peak shows further multiplet splitting. Consequently, the La3*d* region has four distinguishable peaks near 833.4, 837.8, 850.2, and 854.6 eV. The doublet separation of 16.8 eV indicates a trivalent (+3) state of La. At 115 K, La3*d* peaks shift towards higher energy and the multiplet splitting becomes narrower by 0.6 eV, while spin-orbit splitting remains unchanged (16.8 eV). This indicates that in the ferromagnetic state, the oxidation state of La has not changed, while the interaction between unpaired core (2*p*) electron and unpaired valence (3*d*) electron has increased. The XPS core-level of the Ca2*p* region shows two peaks around 345.8 eV and 349.3 eV, which correspond to Ca2$p_{3/2}$ and Ca2$p_{1/2}$, respectively. Similarly, at 115 K, Ca2$p_{3/2}$ and Ca2$p_{1/2}$ peaks were observed at 345.1 eV and 349.6 eV. The doublet separation of 3.5 eV in the Ca2*p* region indicates that Ca exists in the system as a divalent cation (Fig. 2(d)).

Figure 3(a) shows the core-level O1*s* spectra, which consist of two peaks. The first peak at 528.8 eV is characteristic peak of "O^{2-}" ions of the lattice oxygen,[36–39] while peak at 530.9 eV denotes less electron-rich oxygen species[40] and assigned to adsorbed oxygen species, O$_2^{2-}$/O$^-$.[36,41] The significant enhancement observed at 115 K for peak 530.9 eV corresponds to the ionizations of weakly adsorbed species[42] and also the ionizations of oxygen ions with particular coordinates, more specifically integrated in the subsurface. This shows that the sub-surface consists of oxygen ions, which have lower electron density than the "O^{2-}" ions. Normally, these oxide ions can be described as "O$^-$" species or excess oxygen.[43] In the Mn2*p* region, the two peaks observed around 641.4 eV and 653.2 eV correspond to the spin-orbit splitting doublet Mn2$p_{3/2}$ and Mn2$p_{1/2}$, respectively. The doublet separation of 11.8 eV corresponds to either the (+3) valence state or (+4) valence state (Fig. 3(b)). It is also possible that Mn exists in a mixed valence state. To clarify this situation, the peaks of Mn2$p_{3/2}$ and Mn2$p_{1/2}$ have been deconvoluted. The deconvoluted peaks of Mn2$p_{3/2}$ at 641.3 eV and 643 eV (and Mn2$p_{1/2}$ at 653.1 eV and 654.6 eV) represent Mn^{3+} and Mn^{4+}, respectively. This indicates that Mn exists in two valence states (+3 and +4). Similar features
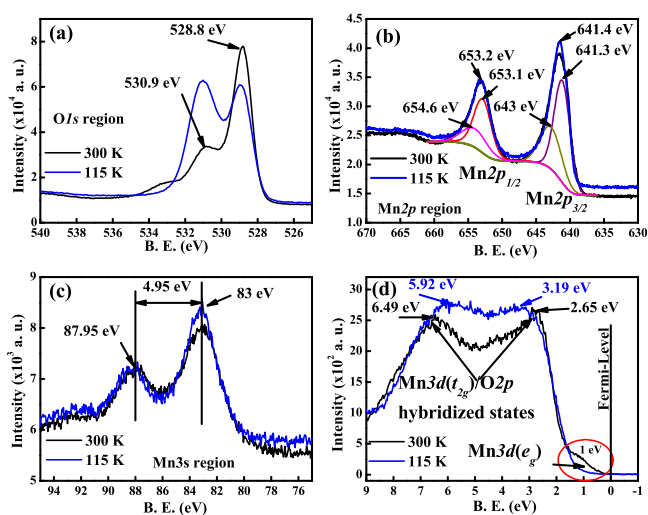
are observed for 115 K spectra of the Mn2*p* region, and there are no significant changes. Further study of the Mn3*s* spectra can provide more information about the Mn valence state (Fig. 3(c)). Mn3*s* spectra show exchange splitting due to the exchange interaction between 3*s*-core holes (created during photoemission process) and 3*d* electrons. Observed exchange splitting energy (ΔE_{3s}) is nearly 4.95 eV for both 300 K and 115 K spectra. ΔE_{3s} is linearly related with the Mn valence (v_{Mn}) by the following equation:[44]

$$v_{Mn} = 9.67 - 1.27\Delta E_{3s}/\text{eV}.$$

The observed exchange splitting $\Delta E_{3s} = 4.95$ eV gives $v_{Mn} = 3.37$, which is consistent with the expected Mn valence (3.35) from the compound formula LPCMO. This confirms that Mn exists in the mixed valence states (+3 and +4) and there is no change in exchange splitting energy below T$_C$.

The valence-band spectra of LPCMO nanocrystals at 300 K (paramagnetic state) and 115 K (ferromagnetic state) are shown in Fig. 3(d). The valence-band is primarily composed of Mn3*d* and O2*p* orbitals and are consequently expected to be more extended than the valence band of transition metals as they contain only 3*d* orbitals. The octahedral crystal-field developed by the six oxygen ions surrounding each Mn ion leads to the splitting of Mn3*d* orbitals into 3$d(t_{2g})$ and 3$d(e_g)$ orbitals. Since the 3$d(t_{2g})$ orbitals point away from the negatively charged oxygen anion, the 3$d(t_{2g})$ band is expected to lie below the 3$d(e_g)$ band. The features between 0 eV and 4 eV primarily correspond to crystal-field split Mn3$d(t_{2g})$ and Mn3$d(e_g)$ states. According to the crystal-field splitting, the feature extended near Fermi-level represents the partially occupied 3$d(e_g)$ band. The spectral features observed between 4 eV and 9 eV are mainly the contribution of O2*p* states. The two most prominent features between 2 eV and 8 eV are due to hybridization of Mn3$d(t_{2g})$ and O2*p* states. Valence band photoemission spectra of the LPCMO nanoparticle recorded at 115 K show two critical differences from the 300 K spectra. First, at 115 K, the energy difference between the two prominent features is about 2.73 eV, while at 300 K, it is about 3.84 eV. This

decrease in hybridized bandwidth between Mn3*d* and O2*p* at 115 K can be understood on the basis of increased double-exchange (DE) interaction in the ferromagnetic state. Second, the electronic states (spectral intensity) near the Fermi-level are suppressed at 115 K in comparison to those at 300 K. It can be seen that ferromagnetic ordering has diminished the area corresponding to the Mn3*d(e_g)* spin-up states, possibly due to suppression of the Fermi surface area in the ferromagnetic state.

In comparison to the XPS valence band, the UPS valence band appears significantly different. The XPS valence band possesses clearly distinguishable Mn3*d* and O2*p* states, while the UPS valence band exhibits its dominant contribution from O2*p* states from 6 eV to 9 eV and suppressed Mn3*d* states (below 3 eV). Low-energy photoelectron emission by ultraviolet photons leads to significantly uneven photoionization cross sections for valence Mn3*d* and O2*p* states.[45] Due to the lower photon energy, UPS shows more sensitivity for lighter atoms, and hence, UPS valence band spectra are mostly dominated by O2*p* states. Figure 4(a) shows that there are no electronic states present until 1.6 eV above Fermi-level for both 300 K and 115 K spectra. The electronic states become effective with a sudden rise in the spectral intensity above 1.6 eV. The feature around 3 eV corresponds to Mn3*d(t_{2g})*, while the tail-like structure below 1.6 eV is due to Mn3*d(e_g)* states. It is remarkable that below T_C, the UPS result also demonstrates suppressed electronic states near the Fermi-level, which is in accordance with the valence band XPS results. For a closer look at the variation in electronic states near the Fermi-level, the high resolution (5 meV) UPS measurements were then taken in the vicinity of the Fermi-level (Fig. 4(b)). From 300 K UPS, it can be clearly seen that the electronic states are nearly absent below 0.5 eV, while spectra measured at 115 K show a total absence of electronic states up to as high as 1 eV above the Fermi-level. This shows that at low temperatures (below T_C), the band gap of the system increases, which is consistent with semiconducting nature.

In conclusion, the electronic structure of the nanocrystalline LPCMO near the Fermi-level was investigated using XMCD, XPS, and UPS measurements. The XMCD result and M-H hysteresis curve show that Mn^{3+} and Mn^{4+} spins are ferromagnetically aligned below T_C. The low temperature (115 K) valence band XPS demonstrates the increased double exchange coupling between Mn3*d* and O2*p* as compared to 300 K spectra. The electronic states near the Fermi-level were found to be suppressed below T_C. The increased

coupling and suppressed electronic states close to the Fermi-level are signatures of an established ferromagnetic state. The valence band UPS also supports the suppression of the electronic states near the Fermi-level below T_C. The absence of the electronic states in the vicinity of the Fermi-level clearly indicates the existence of a wide band-gap in the system, one which increases at low temperature.

[1]Z. G. Sheng, M. Nakamura, W. Koshibae, T. Makino, Y. Tokura, and M. Kawasaki, Nat. Commun. **5**, 4584 (2014).
[2]S. N. Jammalamadaka, J. Vanacken, and V. V. Moshchalkov, Appl. Phys. Lett. **105**, 033505 (2014).
[3]H. Nakayama, M. Althammer, Y.-T. Chen, K. Uchida, Y. Kajiwara, D. Kikuchi, T. Ohtani, S. Geprägs, M. Opel, S. Takahashi, R. Gross, G. E. W. Bauer, S. T. B. Goennenwein, and E. Saitoh, Phys. Rev. Lett. **110**, 206601 (2013).
[4]H. Boschker, J. Kautz, E. P. Houwman, W. Siemons, D. H. A. Blank, M. Huijben, G. Koster, A. Vailionis, and G. Rijnders, Phys. Rev. Lett. **109**, 157207 (2012).
[5]M. Nakamura, Y. Ogimoto, H. Tamaru, M. Izumi, and K. Miyano, Appl. Phys. Lett. **86**, 182504 (2005).
[6]Y. Ogimoto, N. Takubo, M. Nakamura, H. Tamaru, M. Izumi, and K. Miyano, Appl. Phys. Lett. **86**, 112513 (2005).
[7]M. Minohara, Y. Furukawa, R. Yasuhara, H. Kumigashira, and M. Oshima, Appl. Phys. Lett. **94**, 242106 (2009).
[8]M. B. Salamon and M. Jaime, Rev. Mod. Phys. **73**, 583 (2001).
[9]A. P. Ramirez, J. Phys. Condens. Matter **9**, 8171 (1997).
[10]Y. Moritomo, H. Kuwahara, Y. Tomioka, and Y. Tokura, Phys. Rev. B **55**, 7549 (1997).
[11]C. Meneghini, D. Levy, S. Mobilio, M. Ortolani, M. Nunez-Reguero, A. Kumar, and D. D. Sarma, Phys. Rev. B **65**, 012111 (2001).
[12]A. Congeduti, P. Postorino, P. Dore, A. Nucara, S. Lupi, S. Mercone, P. Calvani, A. Kumar, and D. D. Sarma, Phys. Rev. B **63**, 184410 (2001).
[13]P. Postorino, A. Congeduti, P. Dore, A. Sacchetti, F. Gorelli, L. Ulivi, A. Kumar, and D. D. Sarma, Phys. Rev. Lett. **91**, 175501 (2003).
[14]Y. Ding, D. Haskel, Y.-C. Tseng, E. Kaneshita, M. van Veenendaal, J. F. Mitchell, S. V. Sinogeikin, V. Prakapenka, and H.-K. Mao, Phys. Rev. Lett. **102**, 237201 (2009).
[15]H. Kuwahara, Y. Tomioka, A. Asamitsu, Y. Moritomo, and Y. Tokura, Science **270**, 961 (1995).
[16]Y. Tomioka, A. Asamitsu, H. Kuwahara, Y. Moritomo, and Y. Tokura, Phys. Rev. B **53**, R1689 (1996).
[17]Y. Tomioka, A. Asamitsu, Y. Moritomo, H. Kuwahara, and Y. Tokura, Phys. Rev. Lett. **74**, 5108 (1995).
[18]K. Miyano, T. Tanaka, Y. Tomioka, and Y. Tokura, Phys. Rev. Lett. **78**, 4257 (1997).
[19]A. Odagawa, H. Sato, I. H. Inoue, H. Akoh, M. Kawasaki, Y. Tokura, T. Kanno, and H. Adachi, Phys. Rev. B **70**, 224403 (2004).
[20]S. Dong, C. Zhu, Y. Wang, F. Yuan, K. F. Wang, and J.-M. Liu, J. Phys. Condens. Matter. **19**, 266202 (2007).
[21]S. Kumar, G. D. Dwivedi, S. Kumar, R. B. Mathur, U. Saxena, A. K. Ghosh, A. G. Joshi, H. D. Yang, and S. Chatterjee, Dalton Trans. **44**, 3109 (2015).
[22]R. Mahendiran, A. K. Raychaudhuri, A. Chainani, D. D. Sarma, and S. B. Roy, Appl. Phys. Lett. **66**, 233 (1995).
[23]J. H. Lee, K. T. Delaney, E. Bousquet, N. A. Spaldin, and K. M. Rabe, Phys. Rev. B **88**, 174426 (2013).
[24]R. A. Fisher, F. Bouquet, N. E. Phillips, J. P. Franck, G. Zhang, J. E. Gordon, and C. Marcenat, Phys. Rev. B **64**, 134425 (2001).
[25]J. Stöhr, J. Magn. Magn. Mater. **200**, 470 (1999).
[26]B. T. Thole, P. Carra, F. Sette, and G. van der Laan, Phys. Rev. Lett. **68**, 1943 (1992).
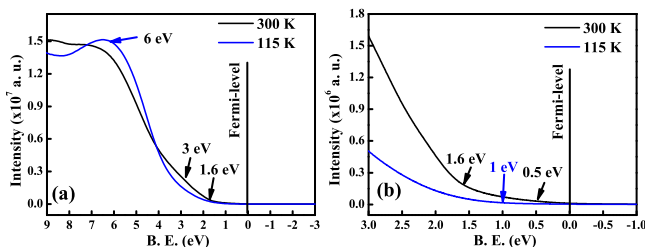[27]P. Carra, B. T. Thole, M. Altarelli, and X. Wang, Phys. Rev. Lett. **70**, 694 (1993).

FIG. 4. (a) Valence band ultraviolet photoemission spectra and (b) high-resolution valence band UPS in the vicinity of Fermi-level at 300 K and 115 K.

[28]D. K. Satapathy, M. A. Uribe-Laverde, I. Marozau, V. K. Malik, S. Das, Th. Wagner, C. Marcelot, J. Stahn, S. Brück, A. Rühm, S. Macke, T. Tietze, E. Goering, A. Frañó, J.-H. Kim, M. Wu, E. Benckiser, B. Keimer, A. Devishvili, B. P. Toperverg, M. Merz, P. Nagel, S. Schuppler, and C. Bernhard, Phys. Rev. Lett. **108**, 197201 (2012).

[29]E. Goering, A. Fuss, W. Weber, J. Will, and G. Schütz, J. Appl. Phys. **88**, 5920 (2000).

[30]F. Li, Y. Zhan, T.-H. Lee, X. Liu, A. Chikamatsu, T.-F. Guo, H.-J. Lin, J. C. A. Huang, and M. Fahlman, J. Phys. Chem. C **115**, 16947 (2011).

[31]D. Yi, J. Liu, S. Okamoto, S. Jagannatha, Y.-C. Chen, P. Yu, Y.-H. Chu, E. Arenholz, and R. Ramesh, Phys. Rev. Lett. **111**, 127601 (2013).

[32]P. Yu, J.-S. Lee, S. Okamoto, M. D. Rossell, M. Huijben, C.-H. Yang, Q. He, J. X. Zhang, S. Y. Yang, M. J. Lee, Q. M. Ramasse, R. Erni, Y.-H. Chu, D. A. Arena, C.-C. Kao, L. W. Martin, and R. Ramesh, Phys. Rev. Lett. **105**, 027201 (2010).

[33]J. J. Kavich, M. P. Warusawithana, J. W. Freeland, P. Ryan, X. Zhai, R. H. Kodama, and J. N. Eckstein, Phys. Rev. B **76**, 014410 (2007).

[34]T. Zhang, X. P. Wang, Q. F. Fang, and X. G. Li, Appl. Phys. Rev. **1**, 031302 (2014).

[35]See A. V. Naumkin, A. K. Vass, S. W. Gaarenstroom, and C. J. Powell for (compilation and evaluation), NIST Standard Reference Database 20, Version 4.1, http://srdata.nist.gov/xps/.

[36]N. Yamazoe, Y. Teraoka, and T. Seiyama, Chem. Lett. **10**, 1767 (1981).

[37]G. U. Kulkarni, C. N. R. Rao, and M. W. Roberts, J. Phys. Chem. **99**, 3310 (1995).

[38]A. F. Carley, M. W. Roberts, and A. K. Santra, J. Phys. Chem. B **101**, 9978 (1997).

[39]J. L. G. Fierro and L. G. Tejuca, Appl. Surf. Sci. **27**, 453 (1987).

[40]N. A. Merino, B. P. Barbero, P. Eloy, and L. E. Cadús, Appl. Surf. Sci. **253**, 1489 (2006).

[41]L. Richter, S. D. Bader, and M. B. Brodsky, Phys. Rev. B **22**, 3059 (1980).

[42]W. Cao, O. K. Tan, W. Zhu, J. S. Pan, and J. Bin, IEEE Sens. J. **3**, 421 (2003).

[43]J. C. Dupin, D. Gonbeau, P. Vinatier, and A. Levasseur, Phys. Chem. Chem. Phys. **2**, 1319 (2000).

[44]E. Beyreuther, S. Grafström, L. M. Eng, C. Thiele, and K. Dörr, Phys. Rev. B **73**, 155425 (2006).

[45]J. J. Yeh and I. Lindau, At. Data Nucl. Data Tables **32**, 1–155 (1985).